A Novel Compliant Mechanism for Converting Reciprocating Translation Into Enclosing Curved Paths

Nilesh D. Mankame

G. K. Ananthasuresh*

University of Pennsylvania,
Department of Mechanical Engineering and
Applied Mechanics,
Philadelphia, PA 19104—6315
e-mail: (nileshdm, gksuresh)@seas.upenn.edu

This paper introduces a novel contact-aided compliant mechanism that uses intermittent contacts to convert a single translatory reciprocating input into two output curves, which intersect to enclose a two dimensional region. Contact interactions endow contact-aided compliant mechanisms with enhanced kinematic and kinetostatic capabilities. The mechanism described in this paper is designed to undergo large deformations repeatedly, without yielding by avoiding flexural joints and by using contacts to obtain the desired deformation. A single-material, joint-free and planar design makes the mechanism easy and economical to fabricate at the macro or micro scales. The design is validated experimentally by manufacturing and testing macro scale prototypes. Two potential applications that motivated this mechanism are also noted. [DOI: 10.1115/1.1759360]

1 Introduction

Conventional rigid-body mechanisms use kinematic joints to produce a wide range of motions. Single-piece compliant mechanisms [1,2], which use elastic deformation of the mechanism body instead of kinematic joints, offer numerous advantages over rigid-body mechanisms in many applications and especially at the micro scale. Two complementary approaches to the design of compliant mechanisms have evolved over the past few decades. The *pseudo-rigid body* method of modeling compliant mechanisms allows traditional rigid-body mechanism synthesis techniques to be applied to the design of compliant mechanisms [3,4]. The topology optimization approach uses techniques from structural optimization to simultaneously determine the mechanism type and link dimensions for compliant mechanisms that perform function or path generation tasks [5,6]. These two techniques for compliant mechanism synthesis have been combined in [7] with the objective of using kinetostatic design requirements as a criterion for choosing an optimum rigid-body mechanism. Motion generation for compliant mechanisms, which involves a shape change along with rigid body motion, has also been accomplished for applications in adaptive structures [8].

Despite significant progress in techniques for their design, existing compliant mechanisms cannot give the wide range of motions that rigid-body mechanisms can provide. The nature of the elastic continuum that constitutes the body of a compliant mechanism, precludes non-smooth motions with a single monotonic input. Barring material nonlinearities such as phase transformations or yielding, and structural instabilities such as buckling, a compliant mechanism will not be able to produce sudden non-smooth changes in motion when subjected to a single continuous input. Therefore, compliant mechanisms are not capable of performing function, path, and motion generation tasks that involve abrupt changes in response. *Contact-aided compliant mechanisms* (CCMs) were introduced in [9] to overcome this fundamental limitation of existing compliant mechanisms. In CCMs, parts of the elastic body of the mechanism intermittently contact each other or a rigid surface. These intermittent contacts endow CCMs with an enhanced kinematic and kinetostatic capability that the compliant mechanisms reported in the literature so far, lack. A CCM that exemplifies this novel feature is the focus of this paper. Two sample applications that motivated the development of this device are described next.

The lack of kinematic joints in compliant mechanisms eliminates wear and backlash related problems. This results in an excellent repeatability of motion [2]. A joint-free or single-piece construction makes their production simple and economical. These characteristics make compliant mechanisms ideal for microsystems applications [10]. However, in some applications that are mechanically challenging for compliant mechanisms, kinematic joints are still indispensable. The transmission in the electrostatic microengine [11] is a notable example. In its best embodiment, the transmission that converts the translatory reciprocating motion of the electrostatic actuator to rotary motion uses at least one revolute joint in addition to the central hub of the output gear. Tanner et al. [12] report that the wear induced by the rubbing of the surfaces at the revolute and sliding joints, causes the failure of the microengine and other micro-machined polysilicon devices rather than the fracture of deformable segments. If a compliant mechanism that could convert reciprocating linear motion to a continuous rotary motion were used in the microengine, revolute joints could be avoided and the engine would have a longer operating life. The mechanism presented in this paper is a stepping stone towards eliminating revolute joints in the microengine and similar applications as it demonstrates a unidirectional tracing of a closed curve with reciprocating translatory input.

In experimental cellular studies, cell harvesting is the term used to describe the process of isolating a single cell of interest from its surrounding tissue. This process is sometimes done manually using micro pipettes or other tools with sharp tips. The operator scribes closed paths into the tissue around the cell to tease it out [13]. This process is laborious and time-consuming. Moreover, much precision and repeatability are needed to avoid damage to the cell being isolated as well as to minimize damage to the surrounding tissue. The size of these organic cells, which ranges from 5 to 100 μm, makes it necessary to use micro tools for this task. A number of commercial robotic cell harvesting systems use various dissection tools (e.g., ultrasonic water jet nozzles, lasers) mounted on multiple precision motion stages [14]. Multiple precision motion stages are necessary to trace two dimensional paths because only linear microactuators with sufficient output force

*Corresponding author.

Contributed by the Mechanisms and Robotics Committee for publication in the JOURNAL OF MECHANICAL DESIGN. Manuscript received Mar. 2003; rev. Jan. 2004. Associate Editor: B. R. Pennock.

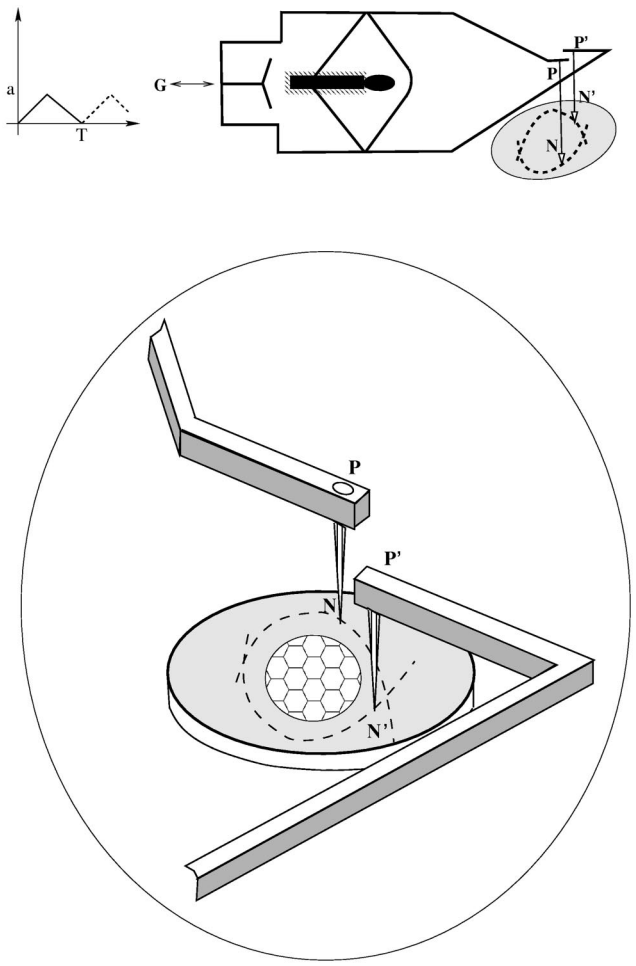

Fig. 1 A schematic representation of the mechanism function

and positioning accuracy are available commercially. The mechanism presented in this paper not only satisfies the primary requirement of the cell harvesting application, but also achieves that with the use of a single linear actuator.

Note that although current fabrication technology allows fabrication of rigid-body mechanisms at the micro scale [15], the use of a micro-scale rigid-body mechanism in place of the presented CCM is infeasible due to the relatively large joint clearances involved in the fabrication of such a mechanism. For example, Mehregany et al. [16] report a joint clearance of 1.2 μm, which corresponds to a total eccentricity of 2.4 μm for a shaft of diameter 20 μm.

The cell harvesting application is chosen as a motivating example for demonstrating the unique kinematic and kinetostatic response of a novel CCM. The mechanism mimics the manual procedure used for cell harvesting, while ensuring high repeatability and accuracy. A schematic describing the mechanism being used for cell harvesting is shown in Fig. 1. The hatched region in the center of the mechanism layout in this figure is anchored to the ground, while a reciprocating translatory input is applied at G. The input is a periodic triangular wave with an amplitude of **a** and a time period of **T**. For the cell harvesting application, the dissection tools **PN** and **P′N′** will be mounted at the output ports **P** and **P′**. The curved paths of the two tools, shown in dashed lines, intersect to enclose a two dimensional region that contains the cell to be excised. The inset at the right of Fig. 1 shows the tools scribing this path into the tissue culture mounted below the mechanism. After this process is repeated a few times, the tissue fragment encircled by the output curves is isolated from the surrounding tissue.

Intermittent contacts between different parts of the mechanism make it possible to get a suitable curvature of the output paths that is required to enclose a sizeable circular area in the application. The contact interactions also ensure that the device is able to exert sufficient output force for the entire range of its motion. It is designed to undergo large deformations without yielding by distributing the bending deformation over larger beam segments instead of concentrating the deformation in short flexural joints. Consequently, the mechanism exhibits distributed compliance rather than lumped compliance [17].

This paper describes the design and analysis of the mechanism and its experimental demonstration using macro-scale prototypes. As the same kinetics and kinematics of elastic deformation hold for compliant mechanisms at the micro scale, the design is unlikely to be substantially different when implemented at the micro scale. The fabrication and testing of a micro scale prototype are beyond the scope of this paper. The rest of this paper is organized in the following manner. Section 2 uses the results of finite element (FE) simulations to elaborate the functioning of the mechanism. Section 3 compares the performance of the design as predicted by nonlinear FE analyses (FEA) with results from testing of macro scale prototypes. The salient features of the device are summarized in section 4. Although a particular application is used as the motivating example in this paper, the concepts embodied in the mechanism design can be applied to any compliant mechanism that is designed to generate precise and complex output paths without using multiple actuators or closed-loop control.

2 Mechanism Simulation

A 3D CAD rendering of the mechanism drawn to scale using I-DEAS© [18] is shown in Fig. 2. The labels on this figure and the schematic of the device shown in Fig. 1 will be used in the discussion that follows.

The part **TT′** of the mechanism in Fig. 2 is anchored to the ground. The actuator is connected to the mechanism at **G**. **P** and **P′** are the output ports of the mechanism. The dissection tools are represented by sharp tips extending below the mechanism body in Fig. 2 marked as **PN** and **P′N′**. When the input port **G** is subjected to a triangular-wave translatory motion along a line joining **G** and **J**, each output port traces a curved path. The curved paths corresponding to the two output ports intersect to enclose a two dimensional region.

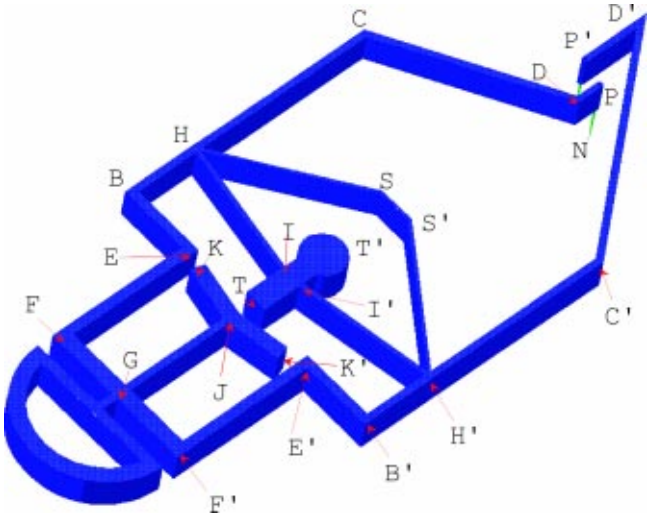

Fig. 2 A three dimensional rendering of the device drawn to scale

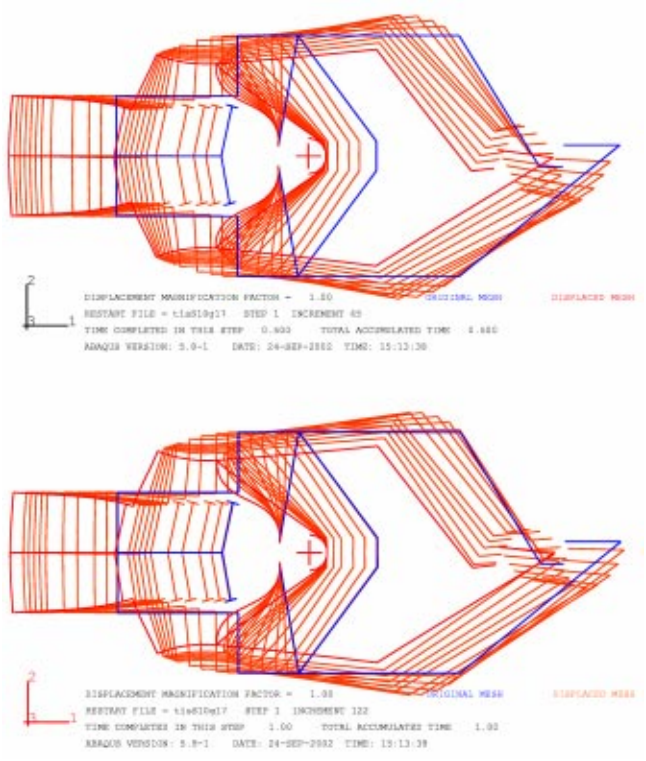

Fig. 3 Nonlinear FE predictions for successive positions of the mechanism during the forward stroke (top) and return stroke (bottom)

The successive positions of the mechanism during the forward stroke and the return stroke are overlaid in Fig. 3. These figures are generated from non-linear FE simulations using a commercial software (ABAQUS©) [19]. The geometry of a macro scale prototype of the mechanism and an elastic material model based on the Young's modulus of polypropylene are used for the simulations. The solid black line (blue) corresponds to the initial or stress-free configuration. The solid dark gray line (red) indicates the configuration at the end of the forward stroke, while the solid lighter gray lines (orange) indicate the intermediate configurations. The colors in parentheses correspond to the full-color electronic version of this document.

The output paths predicted by FEA for the macro scale prototype in the absence of output loads is shown in Fig. 4. The circles mark the positions of **P** and **P′** in the stress-free or initial configuration. The output paths under different output loads, shown in Fig. 5, are described later in this section.

In Fig. 2, the actuator pulls the input port **G** to the left during the forward stroke. Referring to the top frame in Fig. 3, the initial response of the mechanism is largely due to the deformation of the segments **IH**, **I′H′**, **FE** and **F′E′**. The mechanism behaves like an ordinary compliant mechanism during this phase. About half way through the forward stroke, the segment **SS′** contacts the smooth, rigid fixed surface at **T′**. This is closely followed by the point **K** contacting the segment **EF** and **K′** contacting **E′F′**, in that order. These contacts remain closed for the rest of the forward stroke and are re-opened only on the return stroke. These self-contact interactions control the kinetostatic behavior of the mechanism in the following ways:

1. *The paths of the output ports deviate sharply from the initial paths after the contacts close*.
   Without the contacts, continuing deformation of the segments **IH** and **I′H′** could eventually result in an output path that enclosed a two dimensional region. However, such a path would necessarily be elongated and the corresponding deformation would cause material failure at the ends of these segments.
2. *The mode of deformation of the segments* **IH** and **I′H′** *is changed to limit the maximum stress*.
   Most of the pre-contact motion is due to the bending of small end regions of the segments **IH** and **I′H′**. This causes a concentration of stress in these regions, while the remainder of the segments are relatively unstressed. If the segment **SS′** did not contact the point **T′**, the continued deformation of the segments **IH** and **I′H′** in the same mode would lead to material failure at the ends of these segments. The **T′-SS′** contact forces the mode of deformation of the segments **IH** and **I′H′** to change into a more gradual S-shape. This avoids stress concentration at the ends. The change in the mode of deformation, thereby allows the mechanism to continue on the forward (leftward) stroke without exceeding the material strength. The maximum stress in the segments **IH** and **I′H′** at the end of the forward stroke occurs at the points of inflection of the segments, instead of at the ends.

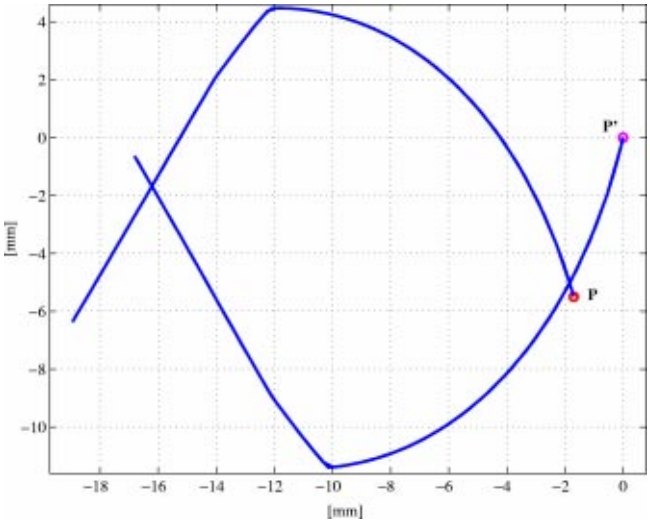

Fig. 4 Paths of the output ports P and P′ from Fig. 1, in the absence of output loads as predicted by non-linear FEA

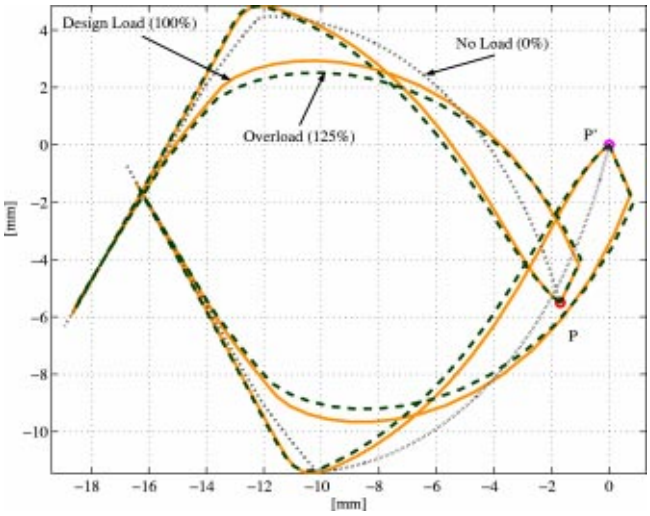

Fig. 5 The paths of the output ports for varying output loads as predicted by nonlinear FEA

3. *The mechanism body is stiffened to retain its ability to deliver useful output force*.
   The input and output ports of the mechanism are located at opposite ends in order to avoid crowding of the work area. However, this design choice compels the motion and force transmission to share a common structural path in the mechanism. These two tasks have conflicting requirements. The mechanism needs to undergo a large deformation to trace a compact two dimensional path that encloses a sizeable area. Hence, the mechanism is designed to have a low inherent stiffness. But a low inherent stiffness limits the amount of output force that can be transmitted to the output ports. The contacts serve to stiffen the structure by limiting excessive deformation. The contacts **K-EF** and **K′-E′F′** prevent further deformation of the segments **EF** and **E′F′**. This can be observed clearly in the top frame of Fig. 3. The reaction due to the **SS′-T′** contact creates anchor points at **H** and **H′**, nearer to the output ports. The contact reaction increases with the continuing leftward motion of the input port **G** and is transmitted through the segments **HS** and **H′S′** to **H** and **H′**. This drives the output ports **P** and **P′** for the rest of the forward stroke by forcing the segments **BC** and **B′C′** to bend.

The input force is gradually reduced to zero during the return stroke to allow the mechanism to spring back to its initial configuration in a controlled manner. The mechanism design is slightly asymmetric to enable the output ports to cross each other's path four times in a complete cycle without interference.

Nonlinear FEA using a linear elastic material model and the data in Table 1 predicts the output paths shown in the Fig. 5. A maximum input force of 33 N and a stroke of 26.7 mm are required to drive the design output load, which has a fixed magnitude of 30 mN per tip. The total excised area is 153 mm^2, while the useful excised area is 112 mm^2 and a circle of 10 mm diameter can be inscribed in the useful excised area for the design load case. The maximum strain in the mechanism over a complete cycle is less than 6%. Comparing this with the minimum yield strain of 8% [20], justifies the choice of a linear elastic material model. Referring to Fig. 5, the useful excised area corresponds to the region at the center that is not crossed by the path of either dissection tool for that load case. The total excised area includes the entire region bounding the useful excised region that is enclosed by the paths of the dissection tools. The useful excised area for the design load predicted by FEA, is 73% of the total excised area. It can be noted that the shape of the enclosed region does not change significantly for variation in the output load from no load to 25% overload.

Unlike the no output load case (see Fig. 4), the return path for both the output ports differs from the corresponding forward path when there is an output load, even if the mechanism is made of a linear elastic material. This is due to variation in the direction of the output load. For the cell harvesting application, the output or cutting load at an output port is the reaction exerted by the tissue on the corresponding dissection tool. The cutting force always opposes the direction of tool motion and for a sharp tool, it is directed along the tangent to the path. In the FE model, the output load is simulated by Coulomb friction in a *gap element*. The gap element is always closed by a normal bias force. Physically, the bias force arises as a reaction from the tissue when the mechanism is positioned over the tissue culture such that the tool presses against the tissue. In addition to capturing the behavior of the output load correctly, this approach makes it easy to vary the magnitude of the cutting load in the FE analysis.

Thermoplastic polymers like polypropylene exhibit a viscoelastic material response. As the experimental validation of the mechanism design is done using macro scale polypropylene prototypes, the viscoelastic material response of polypropylene needs to be included in the simulation model for comparing FE predictions with experimental results. Based on experimental tensile creep data supplied by the manufacturer [21], a simple two element Kelvin-Voigt model was constructed to approximate the viscoelastic response of the material used [22,19]. The experimental data indicates that the apparent Young's modulus of polypropylene decreases by approximately 50% in the first 46.5 s and 14% in the next 46.5 s. Neglecting the inertial effects, a quasi-static simulation of the mechanism behavior using the simple viscoelastic material model for polypropylene yields the output paths shown in Fig. 6 when the mechanism is not driving any output load. A comparision of Figs. 4 and 6 shows that the stress relaxation and creep associated with viscoelastic material response, causes the return path to lie inside the corresponding forward path in any cycle. The forward paths of any cycle lies inside the forward path of the preceding cycle, though the inward shift decreases with time.

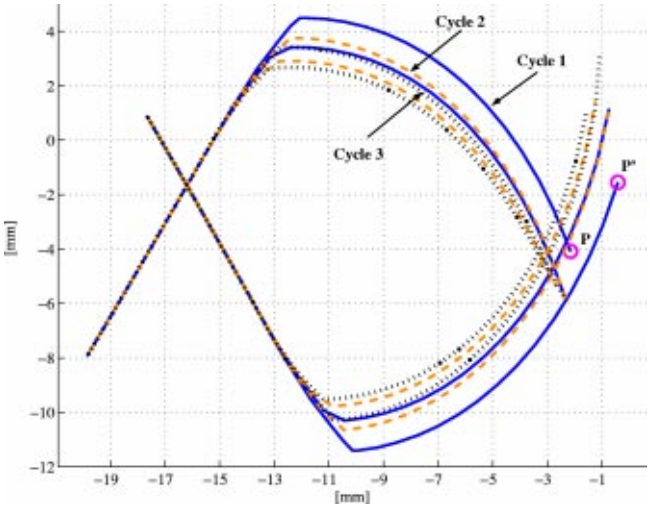

Fig. 6 The predicted paths of the output ports, when the mechanism is run continuously for three cycles at no output load

The conceptual design for this mechanism was based on the kinematic requirements, drawing on prior experience in the design and analysis of compliant mechanisms. The sizing of the relative proportions was done iteratively using nonlinear FEA.

3 Experimental Validation

The ability of the mechanism to repeatably generate output paths that enclose a two dimensional region is verfied by fabricating and testing macro scale polypropylene prototypes. This section covers the experimental observations and relates them to the predictions from nonlinear FEA that were presented in Section 2.

A number of macro scale prototypes ($130\times61\times6.35$ mm) were milled out of a stress-relieved extruded homopolymer polypropylene sheet [23]. Polypropylene was chosen because of many desirable attributes e.g., low cost, easy machinability, high yield strength and high elongation to failure [20]. The dimensions of the prototype and other pertinent details are summarized in Table 1. The experimental setup for the testing of the prototype is shown in Fig. 7. A BasicStamp 2 [24] micro-controller is used in conjunction with a stepper motor (EAD Motors LA23ECKJ-4) to generate the triangular-wave translatory reciprocating actuation for the prototype. The mechanism was run in open loop i.e., without any position feedback. The output is recorded by using sharpened 0.5 mm pencil leads at the output ports **P** and **P′**, which scratch a piece of paper. It is difficult to control the output load precisely in this manner. A closer simulation of the cell harvesting application and a better control over the output load is achieved by placing a bed of compacted powder below the output ports. The powder bed is placed such that the pencil leads at the output port can furrow the bed.

Table 1 Dimensions and parameters for the macro scale prototypes

segment	length	width	segment	length	width
GF	15.0	3.0	**GF′**	15.0	3.0
FE	30.0	2.0	**F′E′**	30.0	2.0
EB	15.0	1.8	**E′B′**	15.0	1.8
BH	15.0	1.5	**B′H′**	15.0	1.45
HC	40.0	1.4	**H′C′**	40.0	1.4
CD	38.4	1.3	**C′D′**	51.6	1.3
DP	5.0	1.3	**D′P′**	13.2	1.3
HI	28.0	0.9	**H′I′**	28.0	0.9
HS	32.8	0.6	**H′S′**	32.8	0.6
JK	12.7	3.0	**JK′**	12.0	3.0
GJ	26.0	1.5	**SS′**	7.3	0.6
GT	47.6	⋯	radius **T′**	4.5	⋯
∠**GJK**	102.0	⋯	∠**GJK′**	102.0	⋯
∠**CHS**	53.5	⋯	∠**C′H′S′**	53.5	⋯
∠**BHI**	80.0	⋯	∠**B′H′I′**	80.0	⋯
∠**HCD**	121.4	⋯	∠**HC′D′**	121.4	⋯

All lengths are in mm and angles are in degrees. The initial Young's modulus for polypropylene is 1448.0 MPa and its Possion ratio is approximately 0.45.

On an average over several runs, the stepper motor completed a cycle with a stroke of 27 mm in 46.5 s. Limitations imposed by the motor prevented the mechanism from being tested at a higher frequency. The tracing of a typical experimentally recorded output path is shown in Fig. 8. The diameter of the largest circle that can be inscribed in the useful excised region is 4 mm. This is less than the value (10 mm) predicted by FEA, as reported in section 2. The deviation can be attributed largely to the following two factors:

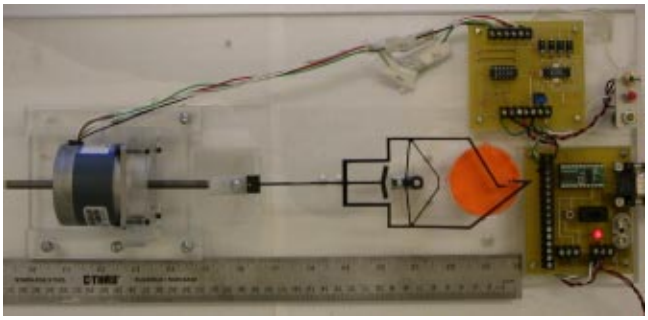

Fig. 7 Experimental setup for testing the macro scale prototype

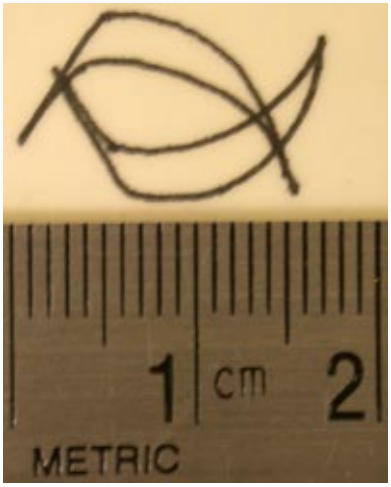

Fig. 8 Experimental recorded output for a macro scale polypropylene prototype

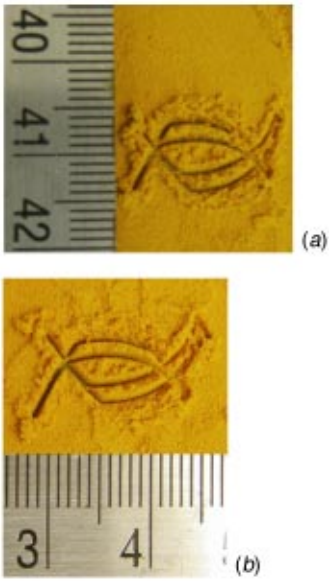

Fig. 9 Experimentally recorded output for a macro scale polypropylene prototype that is run for 10 consecutive cycles (*a*) and the output for another macro scale prototype that is run for 15 consecutive cycles (*b*)

1. The output loads are variable. It is seen in Fig. 5, that overloading the output port causes a reduction in the useful excised area and an increase in the total excised area.
2. Polypropylene is a viscoelastic material.
   As discussed in section 2, the stress relaxation and creep associated with a viscoelastic material response cause an inward shift of the output paths even in the absence of output loads. This shift also contributes to a reduction in the useful excised area.

The smaller relaxation time period (τ) for the simple viscoelastic material model constructed for polypropylene is 33.37 s. As the cycle time (46.5 s) for the experiments is comparable to τ, the influence of the viscoelastic material response on the return path of the mechanism is unavoidable even if only one complete cycle was used to trace the path.

For the cell harvesting application, multiple traversals of the path are needed to tease the region of interest free of the surrounding tissue. Therefore, the prototype was also tested for repeatability of the output paths when subjected to multiple cycles. A compacted powder bed was used to record the output paths for this set of experiments. The results of two different devices that were subjected to 10 and 15 continuous cycles are shown in Fig. 9. It is noted that the forward paths for the second cycle lie *inside* the corresponding forward paths for the first cycle. There is no perceptible shift in the forward paths for the subsequent cycles. The return path remains relatively unchanged for all cycles.

The results of the experiments confirm the ability of the mechanism to repeatably trace output paths that enclose a two dimensional region in response to a single reciprocating translatory input.

4 Salient Features of the Design

On the basis of the performance predicted by the FEA and the results from the experiments on the macro scale prototype, the following salient features of the mechanism design can be discerned.

1. *Single piece construction and simple geometry make the device easy to fabricate.*
   The design has a simple two dimensional geometry, is made

of a single material and has a constant out-of-plane thickness. Therefore, it is easy to fabricate the mechanism even at the micro scale using any microfabrication process that allows one releasable mechanical layer.

2. *Precise and repeatable motion reduces the complexity of the drive electronics*.
   The absence of rigid-body kinematic joints and the associated joint clearances results in a mechanism whose accuracy and repeatability are limited only by the driving actuator. This eliminates the need for monitoring the mechanism output for feedback into the control loop and thus, reduces the complexity of the drive electronics.
3. *The cell harvesting system built around the mechanism is inexpensive*.
   The mechanism requires a single precision microactuator. Moreover, since open loop control can be used, the system comprising the mechanism, its driving actuator and drive electronics will be less expensive than a system of comparable performance that uses multiple coordinated actuators.
4. *The mechanism has a long fatigue life*.
   The mechanism does not use living hinges, flexures or any other form of localized compliance. This, together with the use of contact interactions, results in a more uniform distribution of stresses throughout the mechanism. Therefore, the mechanism has a longer fatigue life.
5. *Absence of sliding contacts minimizes wear at the contact interfaces*.
   All of the contact interactions used by the mechanism rely only on sticking contact. This minimizes contact induced wear. The contact interactions are also localized to three small regions. Lubrication or abrasion resistant coatings (e.g., silicon nitride in micro-machined prototypes) may also be used locally at the contact regions.

Although the mechanism enables a single actuator solution for the cell harvesting application, the path generated by the mechanism is fixed. Moreover, over-loading of the mechanism results in a reduction of the useful excised area. The single actuator based solution threfore, lacks the flexibility of the multiple actuator systems. This is not a major handicap as the mechanism design can be customized for different output loads. Furthermore, the thickness of tissue culture samples used in biological studies is kept small and uniform to enable clear imaging. Therefore, the variation in the cutting load is expected to be small for this application.

The FE simulations and experimental results indicate that the return paths for both the output ports of the mechanism differ from the corresponding forward paths, when the mechanism is driving an output load. Then each output curve is a closed loop by itself. Thus, the mechanism demonstrates that a single-piece elastic structure is capable of repeatedly tracing a closed path unidirectionally, in response to a reciprocating input and a directionally varying output load. The path is nonsmooth and non-circular. But, the topology of the path is similar to the path traced by the end of the crank undergoing continuous rotation in a slider-crank mechanism.

5 Conclusion

A novel single-piece mechanism that uses intermittent contacts to generate a path, which encloses a two dimensional region, was introduced in this paper. Contact interactions enable the output path of mechanism to undergo sharp changes in direction that are necessary to generate a compact path. The contact interactions also helped the mechanism to keep stress low and to maintain sufficient stiffness throughout its working range for ensuring repeatbility of the output path. Experiments on macro scale prototypes ($130\times61\times6.35$ mm) were performed to validate the design of the mechanism.

The mechanism exemplifies a new class of compliant mechanisms: Contact-aided Compliant Mechanisms (CCMs) that can exhibit unique kinematic and kinetostatic responses. CCMs emulate the complex path generation capabilities of rigid-body mechanisms while retaining the scalability, ease of manufacture and repeatability of motion associated with compliant mechanisms. Therefore, they make sophisticated kinematic capability accessible at the micro scale.

Acknowledgments

We wish to acknowledge Mr. B. Balogh, Mr. T. Kientz and Mr. W. Szezesniak for their help in building the experimental setup. We are thankful to the research group of Professor J. Eberwine (Pharmacology, University of Pennsylvania) for sharing their experience with manual cell harvesting. We would also like to thank Professor V. Kumar (Mechanical Engineering and Applied Mechanics, University of Pennsylvania) for introducing us to the cell harvesting application. The financial support of NSF grant (DMI #0200362) for this work is gratefully acknowledged.

References

[1] Midha, A., 1993, *Modern Kinematics-The Developments in the Last Forty Years*, Chapter 9: ''Elastic Mechanisms,'' (A. G. Erdman, ed.), John Wiley and Sons Inc., NY.
[2] Ananthasuresh, G. K., and Kota, S., 1995, ''Designing Compliant Mechanisms,'' ASME Mechanical Engineering, **117**(11), pp. 93–96.
[3] Edwards, B. T., Jensen, B. D., and Howell, L. L., 2001, ''A Pseudo-Rigid Body Model for Initially-Curved Pinned-Pinned Segments Used in Compliant Mechanisms,'' ASME J. Mech. Des., **123**(3), pp. 464–468.
[4] Kimball, C., and Tsai, L.-W., 2002, ''Modeling of Flexural Beams Subjected to Arbitrary End Loads,'' ASME J. Mech. Des., **124**(2), pp. 223–235.
[5] Saxena, A., and Ananthasuresh, G. K., 2001, ''Topology Synthesis of Compliant Mechanisms for Nonlinear Force-Deflection and Curved Path Specifications,'' ASME J. Mech. Des., **123**, pp. 1–10.
[6] Xu, D., and Ananthasuresh, G. K., 2003, ''Freeform Skeletal Shape Optimization of Compliant Mechanisms,'' ASME J. Mech. Des., **125**(2), pp. 253–261.
[7] Saxena, A., and Ananthasuresh, G. K., 2003, ''A Computational Approach to the Number Synthesis of Linkages,'' ASME J. Mech. Des., **125**(1), pp. 110–118.
[8] Saggere, L., and Kota, S., 2001, ''Synthesis of Planar Compliant Four-bar Mechanisms for Compliant Segment Motion Generation,'' ASME J. Mech. Des., **123**(4), pp. 535–541.
[9] Mankame, N. D., and Ananthasuresh, G. K., 2002, ''Contact Aided Compliant Mechanisms: Concept and Preliminaries,'' *Proc. of the 2002 ASME Design Engineering Technical Conferences, Montreal, Canada*, Paper number DETC2002/MECH-34211.
[10] Kota, S., Ananthasuresh, G. K., Crary, S., and Wise, K. D., 1994, ''Design and Fabrication of Microelectromechanical Systems,'' ASME J. Mech. Des., **116**, pp. 1081–1088.
[11] Garcia, E. J., and Sniegowski, J. J., 1995, ''Surface Micromachined Microengine,'' Sens. Actuators, A, **48**(3), pp. 203–214.
[12] Tanner, D. M., Smith, N. F., Irwin, L. W., Eaton, W. P., Helgesen, K. S., Clement, J. J., Miller, W. M., Walraven, J. A., Peterson, K. A., Tangyunyong, P., Dugger, M. T., and Miller, S. L., 2000, ''MEMS Reliability: Infrastructure, Test Structures, Experiments, and Failure Modes,'' Sandia Report, SAND2000-0091.
[13] Eberwine, J., 2002, Private communication.
[14] Willingham, E., 2002, ''Laser Microdissection Systems,'' The Scientist, **16**(10), pp. 42–.
[15] Fan, L.-S., Tai, Y.-C., and Muller, R. S., 1987, ''Pin Joints, Gears, Springs, Cranks and Other Novel Micromechanical Structures,'' *Proc. of Transducers '87*, pp. 849–856.
[16] Mehregany, M., Gabriel, K. J., and Trimmer, W. S. N., 1988, ''Integrated Fabrication of Polysilicon Mechanisms,'' IEEE Trans. Electron Devices, **35**(6), pp. 719–723.
[17] Yin, L., and Ananthasuresh, G. K., 2003, ''A Novel Formulation for the Design of Distributed Compliant Mechanisms,'' Mechanics Based Design of Structures and Machines, **31**(2), pp. 151–179.
[18] Structural Dynamics Research Corporation, I-DEAS Master Series 5, mechanical CAE/CAD/CAM software, 1997.
[19] Abaqus Inc. Abaqus/Standard version 5.8, User's Manual, 1998.
[20] Maier, C., and Calafut, T., 1998, *Polypropylene, The Definitive User's Guide and Databook*, Plastics Design Library, Norwich, NY.
[21] Poly Hi Solidur Inc., 2003, ''Tensile Creep Data for PROTEUS Homopolymer Polypropylene,'' Private communication, February.
[22] Ferry, J. D., 1980, *Viscoelastic Properties of Polymers, Third Edition*, John Wiley and Sons, Inc.
[23] Poly Hi Solidur Inc., Technical information for PROTEUS natural homopolymer polypropylene. Fort Wayne, Indiana 46809.
[24] Parallax Inc., 2002, *BASIC Stamp Version 2.0 User's Manual.*, Rocklin, CA 95765.